Coral Reefs (2014) 33:1167–1178
DOI 10.1007/s00338-014-1205-7

REPORT

The large-scale influence of the Great Barrier Reef matrix on wave attenuation

Shari L. Gallop · Ian R. Young · Roshanka Ranasinghe · Tom H. Durrant · Ivan D. Haigh

Received: 18 April 2014 / Accepted: 25 August 2014 / Published online: 10 September 2014

Abstract Offshore reef systems consist of individual reefs, with spaces in between, which together constitute the reef matrix. This is the first comprehensive, large-scale study, of the influence of an offshore reef system on wave climate and wave transmission. The focus was on the Great Barrier Reef (GBR), Australia, utilizing a 16-yr record of wave height from seven satellite altimeters. Within the GBR matrix, the wave climate is not strongly dependent on reef matrix submergence. This suggests that after initial wave breaking at the seaward edge of the reef matrix, wave energy that penetrates the matrix has little depth modulation. There is no clear evidence to suggest that as reef matrix porosity (ratio of spaces between individual reefs to reef area) decreases, wave attenuation increases. This is because individual reefs cast a wave shadow much larger than the reef itself; thus, a matrix of isolated reefs is remarkably effective at attenuating wave energy. This weak dependence of transmitted wave energy on depth of reef submergence, and reef matrix porosity, is also evident in the lee of the GBR matrix. Here, wave conditions appear to be dependent largely on local wind speed, rather than wave conditions either seaward, or within the reef matrix. This is because the GBR matrix is a very effective wave absorber, irrespective of water depth and reef matrix porosity.

Keywords Offshore reef · Coral · Wave dissipation · Satellite altimetry · Wave transmission

Introduction

Wave breaking occurs at the seaward edges of reefs, then as waves cross the reefs, bottom friction further reduces

Communicated by Geology Editor Prof. Chris Perry

S. L. Gallop (✉) · I. D. Haigh
Ocean and Earth Science, National Oceanography Centre, University of Southampton, European Way, Southampton SO14 3ZH, UK
e-mail: S.Gallop@soton.ac.uk

I. D. Haigh
e-mail: I.D.Haigh@soton.ac.uk

I. R. Young · R. Ranasinghe
Research School of Earth Sciences, Australian National University, Canberra, ACT 0200, Australia
e-mail: ir.young@anu.edu.au

R. Ranasinghe
Department of Water Engineering, UNESCO-IHE, PO Box 3015, 2601 DA Delft, The Netherlands
e-mail: r.ranasinghe@unesco-ihe.org

R. Ranasinghe
Harbour, Coastal and Ocean Engineering, Deltares, PO Box 177, 2600 MH Delft, The Netherlands

T. H. Durrant
Centre for weather and climate research, Bureau of Meteorology, GPO Box 1289, Melbourne, VIC 3001, Australia
e-mail: T.Durrant@bom.gov.au

I. D. Haigh
School of Civil, Environmental and Mining Engineering, UWA Oceans Institute, The University of Western Australia, 35 Stirling Highway, Crawley, WA 6009, Australia

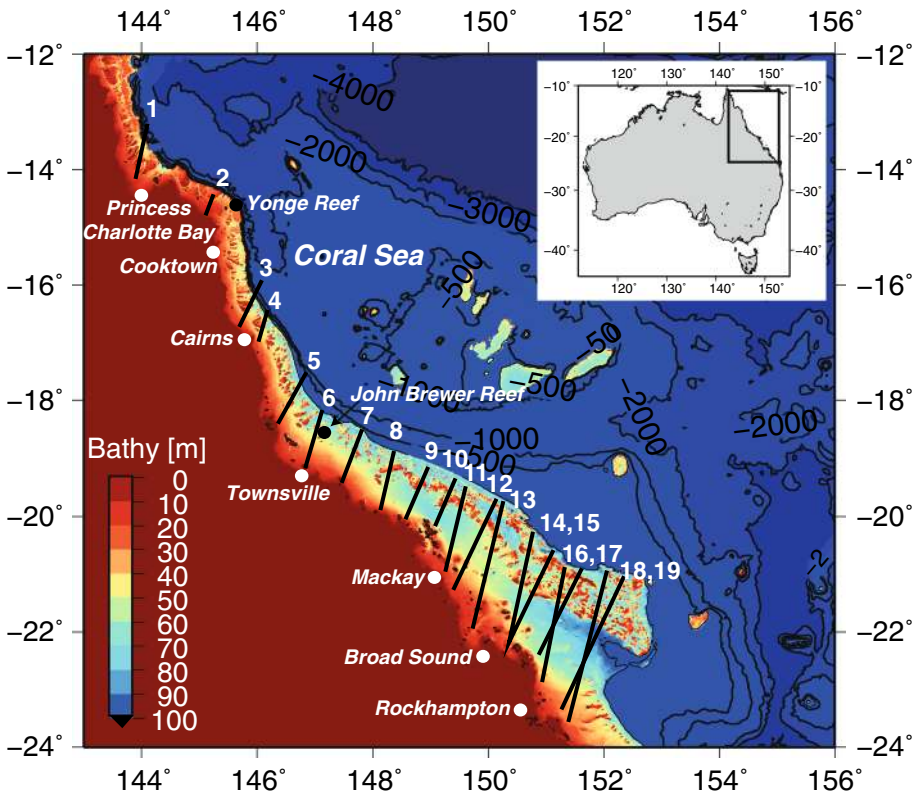

Fig. 1 Great Barrier Reef bathymetry (derived from Beaman 2010), and the 19 altimeter tracks that were analysed, with a total of 2,003 passes

wave height (Young and Hardy 1993). As waves break and attenuate, the mean water surface elevation increases (set-up), driving currents (Longuet-Higgins and Stewart 1962) and reef circulation (Hamner and Wolanski 1988; Pickard et al. 1990; Symonds et al. 1995; Angwenyi and Rydberg 2005). Such currents have implications for the transport of sediments, pollutants, nutrients, plankton, and larvae (Lowe et al. 2005). Wave exposure also plays a role in reef ecology through its relationship to the community structure of coral reefs (Dollar 1982), and is instrumental in sand bank and island formation (Gourlay 1988, 1990), shoreline stability (Young and Hardy 1993), and engineering design and operation.

The Great Barrier Reef (GBR) is the largest coral reef system in the world and has almost every form of reef morphology found elsewhere, apart from atolls (Hopley et al. 2007). The GBR consists of a 'reef matrix', created by thousands of individual reefs, separated by spaces through which wave energy can propagate. The ratio of spaces between individual reefs to total reef area can be described as the 'porosity' of the reef matrix. On the GBR, waves can propagate through the reef matrix without completely dissipating, leading to transmission of significant amounts of wave energy (Hardy and Young 1996). This is unlike mainland beaches and fringing reef-lagoon systems (Hardy and Young 1996), where waves generally terminate and energy is dissipated or transformed into changes in water level and currents (e.g., Lugo-Fernández et al. 1998; Storlazzi et al. 2004; Lowe et al. 2009; Gallop et al. 2012). Little is known about how the porosity of reef matrices influences wave attenuation.

There is reasonable knowledge of wave conditions offshore of the GBR, but data within, and in the lee of the reef matrix are scarce (Hopley et al. 2007). There have been a few local studies where in situ wave measurements were acquired within the GBR matrix. Seaward of the GBR, typical wave periods are approximately 10 s (Wolanski 1986); in the lee, Murray and Ford (1983) found a bimodal sea state consisting of a low amount of energy at 10 s and much more energetic, shorter period sea. It was suggested that the 10 s low energy was from waves that penetrated through the reef matrix, while high-energy sea was locally generated in the lee of the reef. Young (1989) and Hardy et al. (1990, 1991) found that over John Brewer Reef in the central GBR, and Yonge Reef in the northern GBR (Fig. 1), there were dramatic decreases in wave height and energy, and periods longer than 8 s were fully attenuated. It was also suggested that wave height over reefs is determined largely by the depth of reef submergence, i.e., waves are depth–limited. However, there was significant scatter in the data, indicating that other factors are also important.

Young and Hardy (1993) used a combination of numerical models and measurements from four in situ instruments during a tropical cyclone. They found that cyclone-generated waves seaward of the GBR matrix had significant wave heights (H_s) of ~10 m, which were attenuated to 6 m in the lee of the matrix. Wave conditions over individual reefs were strongly modulated by the tide, but not in spaces within the reef matrix (Young and Hardy 1993). Results also suggested that although not all wave energy was dissipated by wave breaking at the seaward edge of reefs, most of the remaining energy was dissipated due to bottom friction over reefs (Young and Hardy 1993). Similar processes of wave attenuation have been observed on fringing reefs, such as in Hawaii (Lee and Black 1979; Gerritsen 1981), Japan (Kono and Tsukayama 1980), the Caribbean (Roberts 1981), and Guam (Pèquignet et al. 2011).

In this research, it was hypothesized that wave attenuation across the GBR is a function of (1) the porosity of the reef matrix, (2) the depth of reef submergence, and (3) local wind speed. To investigate this, it was necessary to have measurements of wave heights across different sections of the reef matrix during a range of wave, water level, and wind conditions. In order to cover this broad range of parameters, satellite altimeter data of H_s were the most practical data source that provides abundant information on the spatiotemporal variability of wave heights.

Materials and methods

Study area

The GBR is an offshore reef matrix that extends 2,300 km alongshore (Hopley et al. 2007), with more than 2,900 individual reefs (Hopley et al. 1989; Fig. 1). The average area of individual reefs is 6.9 km^2, and the total reef area is 20,055 km^2 (Hopley et al. 1989). In the north, reefs are predominantly two-dimensional (i.e., very narrow in the cross-shore direction) and create almost a complete barrier to incident waves (Young 1989). Further south, the reef matrix is more three-dimensional and porous, with porosity decreasing at the southern end. Wave propagation through the reef matrix is influenced by spectral modification of waves propagating across individual reefs, two-dimensional processes such as diffraction and refraction, and the porosity of the reef matrix (Young 1989). The wind and wave climate is strongly seasonal, with a summer-monsoonal climate. During April to September, waves are generated mainly by the persistent southeasterly winds, while during October to March, variable northerly winds dominate (Gourlay 1990).

Satellite altimeter data

Altimeter data were extracted from seven satellite missions: Topex-Poseidon, ERS1 and 2, GFO, Jason1 and 2, and Envisat. These data spanned September 1992 to May 2008, with a total of 5,205 passes over the GBR. Topex-Poseidon, Jason1, and Jason2 had a repeat cycle of 10 days, at 1,336 km altitude; ERS1, ERS2, and Envisat had a repeat cycle of 35 days at 800 km altitude; while GFO had a repeat cycle of 17 days at 800 km altitude. Only passes heading in a southwest–northeast orientation (descending) were used, because these are approximately perpendicular to the GBR matrix. In addition, only tracks with at least 30 repeat passes, and those that crossed the reef matrix at an angle of 70–110° (near perpendicular) compared to the local orientation of the matrix, were utilized. This resulted in 19 tracks with a total of 2,003 passes (Fig. 1). One H_z H_s and wind speed 10 m above the sea surface derived from these passes were used.

Altimeters measure H_s within a circular footprint, the size of which varies with sea state, altimeter altitude, and pulse duration (Chelton et al. 1989). For example, the Topex–Poseidon footprint diameter increases from 8 km during calm sea, to 11 km for H_s of 15 m. Altimeters measure at 20 Hz and travel with a ground speed of around 6–7 km s^{-1}. These measurements are usually averaged for oceanographic applications to 1 Hz to reduce noise. Therefore, depending on the sea state and the size of the footprint, a single 1 Hz-averaged measurement of H_s would typically be an average of 20 successive footprints over an area 10 km wide and 17 km long.

In close proximity to reefs and coasts, altimeter data frequently contain spikes. In previous studies, such errors have been removed by a combination of the application of land masks and automatic outlier removal algorithms (Young 1999; Zieger et al. 2009; Young et al. 2011). However, these techniques typically filter the data too aggressively, removing much valuable and reliable data close to reefs, which are required for the present research. Thus, the raw satellite altimeter passes were visually checked for obvious data errors and regions where data spikes were present were manually excluded, as was done by Young et al. (2013). In the present application, interest is in the attenuation of the altimeter-measured wave height across the reef matrix. As a result, the raw values of significant wave height provided by the respective satellite agencies were used rather than any post-processed calibrations (Zieger et al. 2009).

Bathymetry

Bathymetry along the satellite passes was obtained from Project 3DGBR (Beaman 2010). This bathymetry has

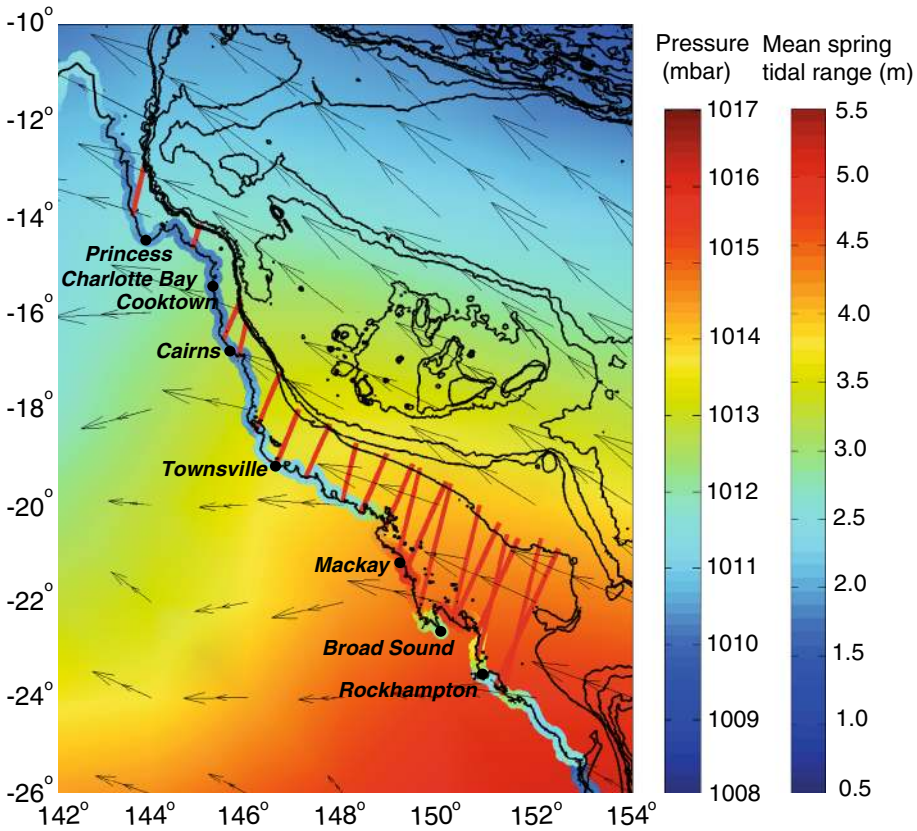

Fig. 2 Background shows mean atmospheric pressure (*colour*) and mean wind direction (*arrows*) between 1992 and 2008, derived from the NCEP global reanalysis. The strip along the coast shows the mean spring tidal range between 1992 and 2008. Bathymetry contours are shown every 100 m, and the 19 satellite tracks for analysis are shown in *red*

resolution of 0.001-arc degrees (100 m), with a horizontal datum of WGS84, and a vertical datum of mean sea level (MSL). It is a combination of multi-beam, single-beam, lidar, and satellite bathymetry collected between 1971 and 2010.

Water level

Hourly water levels relative to MSL at the same times and locations as the satellite passes were obtained from a numerical hydrodynamic hindcast (Haigh et al. 2014a, b). This hindcast utilized a depth-averaged tide and surge model, using the Danish Hydraulic Institute's (DHI) Mike21 model. A flexible mesh was used with resolution of 20 km at the open boundaries around Australia, gradually increasing to a resolution of 10 km near the coast. The model was forced with meteorological fields obtained from the US National Center for Environmental Prediction's (NCEP) global reanalysis (Kalnay et al. 1996; Kistler et al. 2001; Fig. 2).

Tides are mixed with both diurnal and semidiurnal components, except in Broad Sound (Fig. 2) where they are diurnal only (Hopley et al. 2007). Reefs may be exposed at low spring tides, while at high tide can be submerged by several metres (Symonds et al. 1995). North of 18°S, mean spring tidal range is <2 m, then starts to increase around Townsville to 2.5 m (Fig. 2). From here, tidal range increases to more than 6 m in the vicinity of Broad Sound. South of 23°S, tidal range decreases. This has implications for the spatial variability in the depth of reef submergence.

Wave height

The dominant wave direction (southeasterly) and the satellite tracks (southwest–northeast) have different orientations. Therefore, the analysis undertaken here would be much simpler if it were possible to assume that deep water wave heights were relatively spatially invariant along the length of the GBR matrix. To investigate whether this assumption could be made, wave data were extracted along the 100 and 2,000 m contours from a 30-yr wave hindcast using WAVEWATCH III (Tolman 1991, 2009). The model covered the period from 1979 to 2009 (Durrant et al. 2014) and was forced with Climate Forecast System Reanalysis surface winds (CFSR; Saha et al. 2010). The model was run on a 0.4 by 0.4° global grid, with a series of nested grids of 10 arc min down to 4 arc min (~7 km) around the Australian coast (Fig. 3). These grids were two way-nested following Tolman (2008), resulting in a completely self-consistent means of locally increasing resolution,

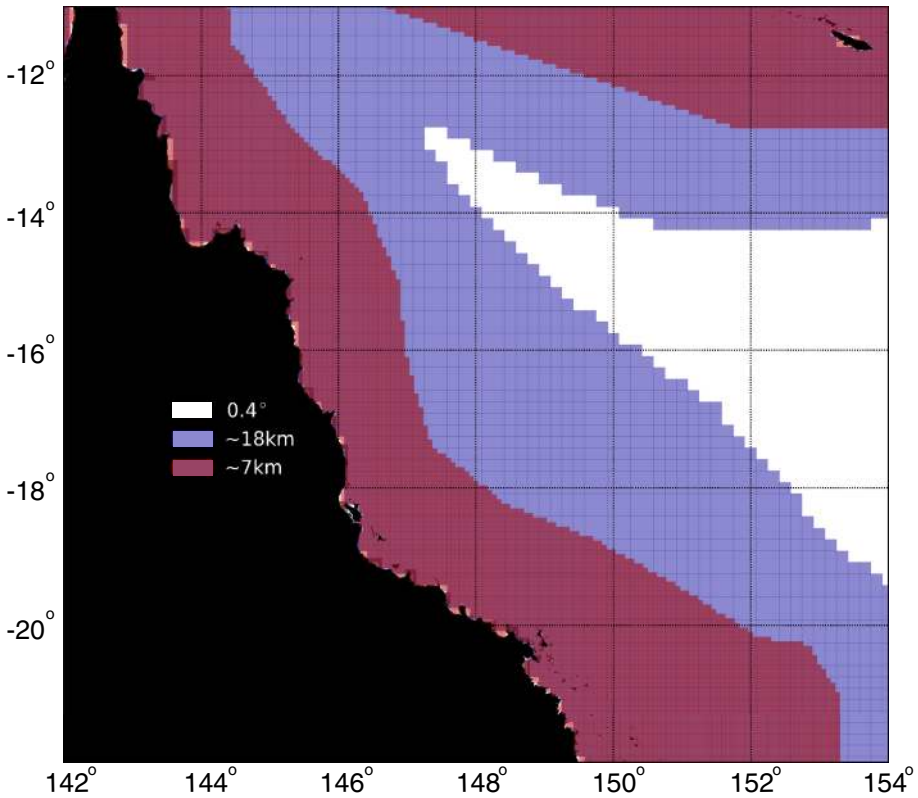

Fig. 3 Nested wave model grid resolutions around the region of interest: the Great Barrier Reef, from Durrant et al. (2014)

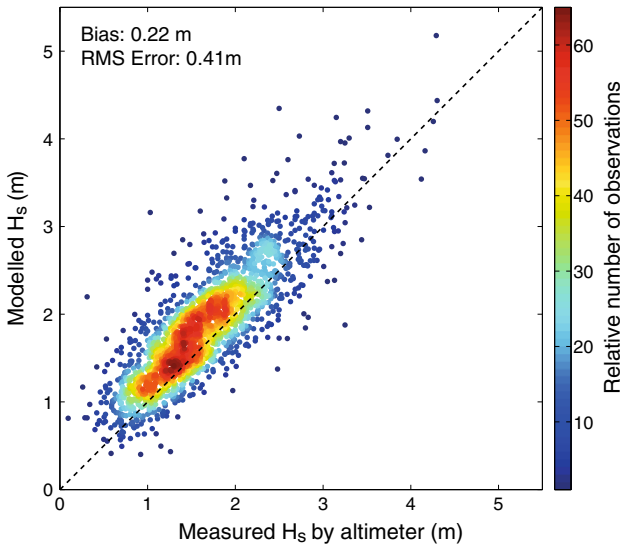

Fig. 4 Comparison of modelled and measured (satellite altimeter) H_s seaward of the reef matrix. *Dashed line* is 1:1

providing data of significantly higher quality and resolution than was previously available. The mean and standard deviation of H_s were calculated for the full 30 years covered by this hindcast. A comparison between offshore H_s measured by the altimeters and the model was in good agreement with close to a 1:1 correlation (Fig. 4). There was only a slight bias by the model of 0.22 m.

A typical barrier reef consists of a forereef sloping up to the reef crest; a lagoon; and a reef flat (Lowe et al. 2005). Individual reefs at the edge of the GBR shelf tend to have steep offshore-facing edges, so waves have little interaction with the seabed even a few 100 m from the forereef (Hopley et al. 2007). Most waves break over the reef crest, then can subsequently reform where there is a lagoon (Gourlay 1990), and break closer to shore (Fig. 5b).

Wave attenuation was estimated over the segment of reef matrix that was closest to the coast by extracting H_s measured by satellite altimeters, at three locations along each satellite pass:

1. *offshore* where depth seaward of the reef matrix first exceeded 100 m to MSL;
2. *within the reef matrix* at the subsequent satellite measurement after the offshore location;
3. *lee of the reef matrix* at the furthest measurement landward of the reef matrix where the depth becomes less than 40 m (Fig. 5).

Linear regression showed that distance across the reef matrix between the extraction points offshore and in the lee of the matrix did not have a statistically significant influence on the magnitude of wave attenuation.

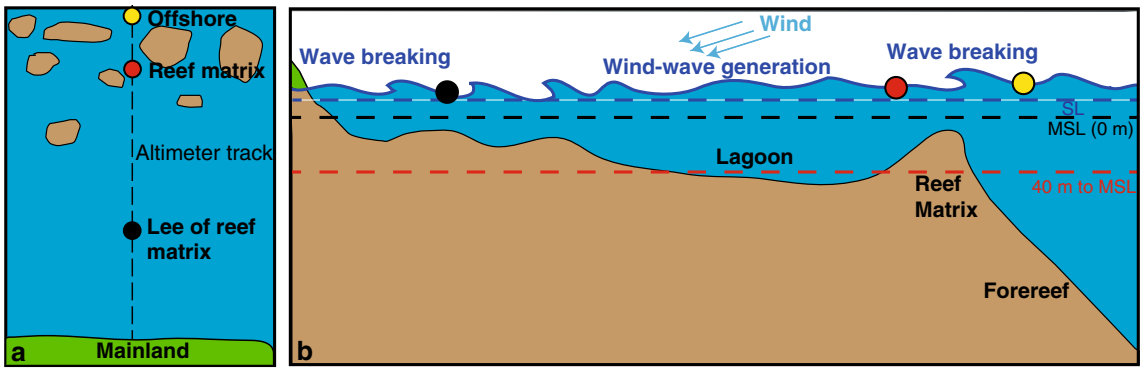

Fig. 5 Schematic of a typical cross section of the GBR matrix; showing example locations of H_s extraction from satellite altimeters; MSL is mean sea level and SL is instantaneous sea level. **a** A plan view; and **b** the profile view. As data from the altimeters represent an average over an area typically 10 km by 17 km, wave attenuation across individual reefs is not resolved. Rather, as shown in the figure, interest is focused on attenuation across the GBR matrix which is composed of numerous individual reefs

Porosity index of the reef matrix

The porosity of the reef matrix was represented by a 'porosity index'. This index was generated based on the volume of water compared to the volume of reef above the 40 m depth contour (Fig. 5b), between the forereef (100 m depth) and the lee of the reef. A range of depths were tested from 0 to 100 m with respect to MSL. Sensitivity testing showed that using 40 m gave the greatest range of porosities across different sections of reef, and is also a level which distinguishes between individual reefs, the regions between reefs, and the GBR lagoons in the lee of the reef matrix. In addition, this corresponds to the approximate depth where waves start to 'feel the bottom'. The mean incident wave period in the GBR region from the hindcast was 8.1 s, with standard deviation of 1.4 s. According to linear wave theory (Dean and Dalrymple 1991), the corresponding deep water wave length for an 8 s wave is around 100 m; waves start to 'feel the bottom' when water depth is half the wave length, which is 50 m depth for a wave with 100 m wave length.

A porosity index of 0 indicates that the entire volume above 40 m was reefs or seabed (i.e., 0 % porous), while 1 specifies that there were no reefs or seabed above 40 m depth (i.e., 100 % porous). This index was calculated for the length of the GBR, in cells that were 10 km wide (corresponding to the approximate width of the satellite footprints), extending from the coast to the 100-m contour. The index was developed to understand mean wave attenuation over the GBR.

Future research is planned to understand more about the permeability of the reef matrix, which will be determined not just by the porosity index, but likely also the angle of incident wave approach, and the effectiveness of the individual reef geomorphology at dissipating waves, which depends in part on reef slope and spatial continuity.

Results

Offshore incident waves

The offshore wave climate of the GBR consists largely of southeasterly swell generated in the Coral Sea (Fig. 1), and occasionally, cyclone-generated waves during December to April (summer; Hopley et al. 2007). Mean, peak wave period (T_p) is generally between 8 and 9 s offshore of the GBR, and from the forereef (around the 100 m contour) decreases to between 6 and 7 s, likely due to the local generation of wind waves (Fig. 6a). The mean incident wave direction is southeasterly (Fig. 6b). Therefore, the offshore wave height relevant to the wave attenuation along a given satellite pass may be quite different to the offshore wave height extracted from the pass itself. That is, the waves measured by the altimeter seaward of the GBR may not propagate along the altimeter track. Rather, waves measured by the altimeter landward of the GBR matrix could have propagated from a seaward point to the southeast. However, if it can be assumed that the wave field seaward of the GBR does not change significantly; then, the discrepancy in direction of the satellite track and offshore waves will not introduce significant error. To investigate whether this is the case, numerical model-derived H_s along the 2,000 and 100 m depth contours offshore of the GBR matrix were analysed. For most of the 2,000 m contour, mean H_s varied between 1.6 and 1.8 m; and SD was between 0.7 and 0.75 m. From 12 to 14°S mean H_{s100} decreased from 1.7 to 1.2 m (Fig. 6c), and SD decreased from 0.7 to 0.5 m (Fig. 6d). From 14 to 15°S, mean H_{s100} increased from 1.2 to 1.7 and SD also increased from 0.5 to 0.7. From 15°S, there was a decrease in mean H_{s100} to 1.5–1.6 m and SD was between 0.65 and 0.7 m. South of 21°S, mean H_{s100} increased to 1.75 m.

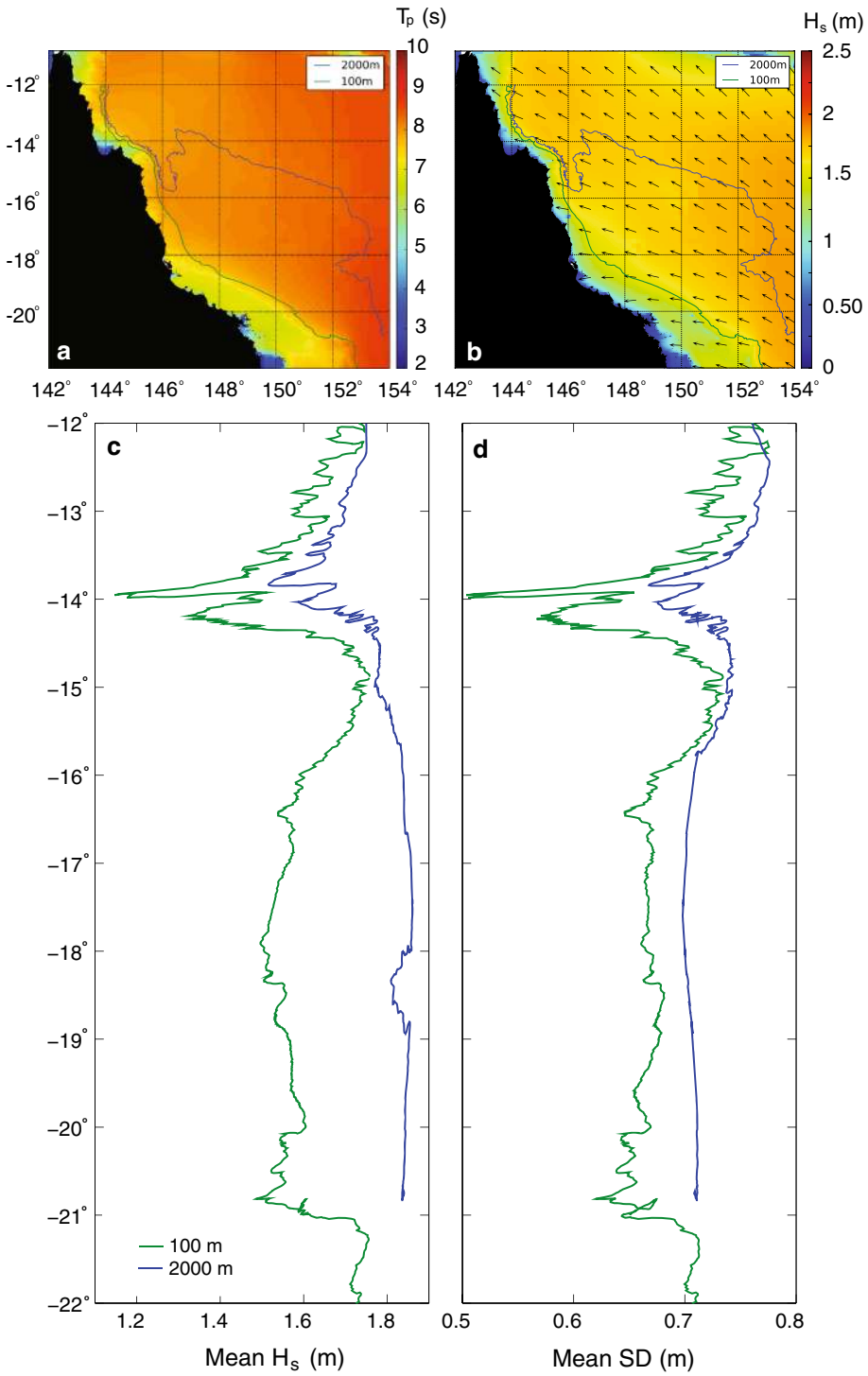

Fig. 6 **a** Mean T_p from the model; **b** mean H_s from the WAVEWATCH III hindcast (*colour*) and mean incident wave direction (*arrows*); **c** H_s along the 100 and 2,000 m contours (H_{s100} and H_{s2000}); and **d** standard deviation between 1992 and 2008

The abrupt decrease in mean H_{s100} and H_{s2000} around 14 to 15°S is due to a change in the local orientation of the coast and the reef matrix. For most of the GBR, the mainland and the reef matrix faces the northeast. However, from 14 to 15°S (Princess Charlotte Bay, Fig. 1), the orientation becomes more northerly, so is largely sheltered from the incident southeasterly waves (Fig. 6b). In this area, the forereef is very steep and the 100 m and 2,000 m contours lie up to 8 km apart, compared with up to 500 km in the central GBR (Fig. 1). Therefore, the sheltering effect of the coastal orientation is evident in incident H_s along the 100 and 2,000 m contours. No satellite tracks were analysed from this section of coast due to the large discrepancy between the orientation of the coast and reef matrix with

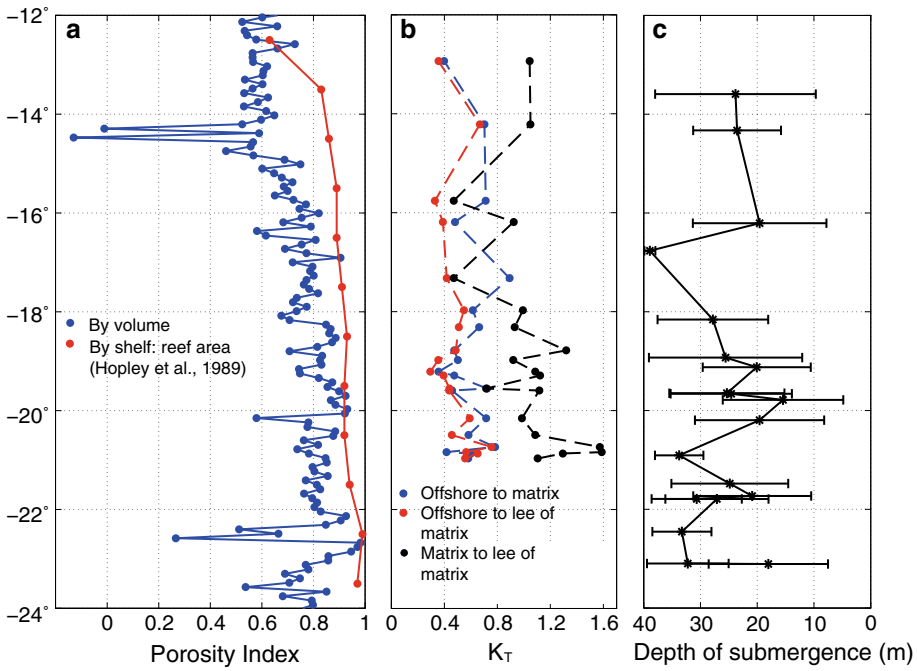

Fig. 7 **a** Porosity index every 10 km alongshore between the coast and 100 m contour; **b** wave transmission coefficient calculated as in Nelson and Lesleighter (1985) at the 40 m contour; and **c** mean (*star* and *lines*) and standard deviation (*bar*) of submergence to mean sea level at the edge of the reef matrix (reef crest)

altimeter passes (Fig. 1). However, for the remainder of the GBR matrix, within 1° latitude (~111 km) regions, mean incident H_{s2000} varied by <2 cm, and mean H_{s100} by <5 cm. Therefore, assuming that the measured offshore incident H_s from the satellite tracks represents the wave conditions seaward of the GBR which would propagate across the reef matrix, is likely to result in errors of H_s of only a few cm.

Porosity of the reef matrix

There is a trend of increasing reef matrix porosity from north to south (Fig. 7a). In the north, porosity averages approximately 0.6 (i.e., 60 % porous) where the shelf is narrower than 8 km. From 15°S as the shelf widens, porosity starts to increase, and in the central GBR is mostly between 0.7 and 0.95. In the south, the shelf is up to 300 km wide, and there is an extensive lagoon that is more than 200 km wide in the far south. This lagoon leads to high porosities of generally more than 0.8. The trend of porosity is similar to the much lower resolution (1° latitude) estimate of the area of shelf to reef calculated by Hopley et al. (1989; Fig. 7a), but here calculated at much higher resolution. The porosity index indirectly reflects the geomorphology of individual reefs. For example, according to Hopley et al. (1989), north of 16°S, planar reefs are common and associated with extensive reef flats and a lack of lagoons, leading to lower porosity in the north. Crescentic reefs dominate the central GBR between 14 and 22°S, with an open back reef area and lagoons, reflected in the increasing porosity index in the area. Lagoonal reefs are mainly restricted to south of 19°S, and in combination with the wide shelf and extensive lagoons, leads to the highest porosity index in the southern GBR.

Reef submergence

The depth of submergence of the reef matrix along each of the altimeter tracks is shown in Fig. 7c. Although successive altimeter passes are nominally along the same track, the exact tracks vary within several km, reflected in the standard deviation of bathymetry. The mean depth of reef submergence varied between 15 and 45 m, with significant variability between passes and no clear trend along the length of the GBR. It is not surprising that there is no apparent trend in submergence along the length of the GBR.

Coral reefs tend to grow up to the low tide level, and hence, one would initially expect a similar depth of submergence at all locations. This relationship is reflected in the positive correspondence between tidal range, and the variation of reef submergence (represented by standard deviation). However, the correlation coefficient (r) is relatively low at 0.22 and is not statistically significant, with a probability value (p) of 0.37 (Fig. 8a).

Wave transmission

Reef geomorphology has a strong influence on wave attenuation and the development of locally generated wind

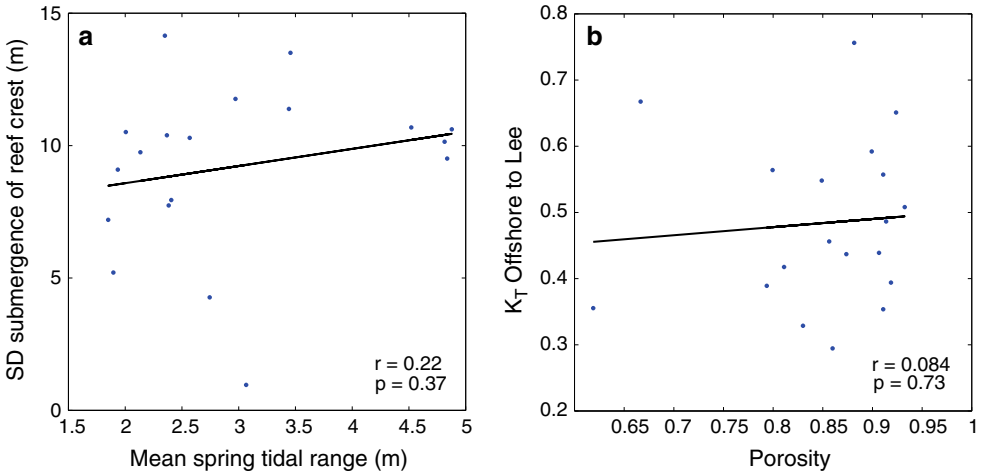

Fig. 8 Relationship between **a** mean spring tidal range and standard deviation (SD) of reef crest submergence to MSL; and **b** porosity and wave transmission (K_T) matrix to lee. r is the correlation coefficient and p is the probability value

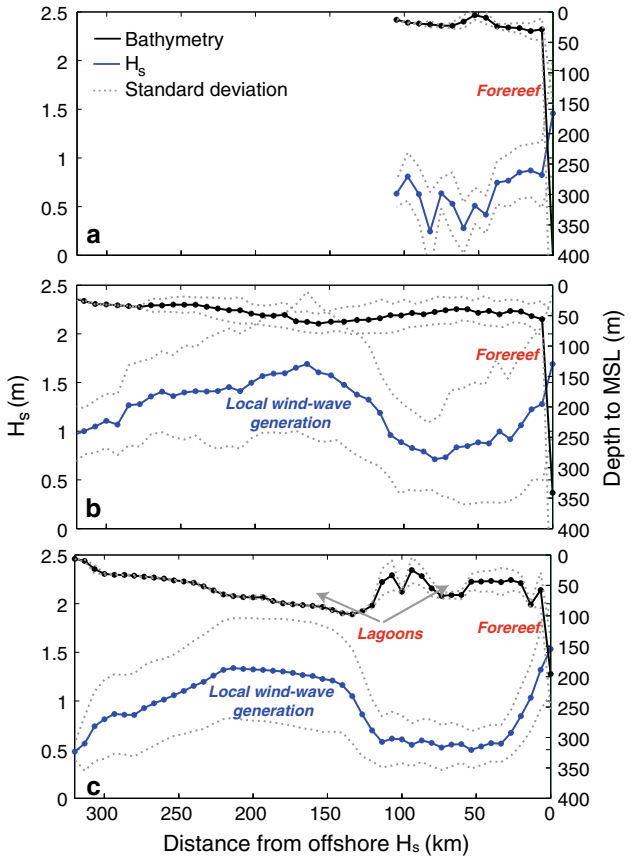

Fig. 9 Mean bathymetry (*black*) and mean H_s (*blue*) along tracks as a function of distance from the offshore H_s extraction location along tracks **a** 1, **b** 6, and **c** 14. *Grey dotted lines* show standard deviation

waves. This is demonstrated in Fig. 9 which shows the mean values of H_s averaged over all passes along tracks 1, 6, and 14 in the northern, central, and southern GBR, respectively (see Fig. 1 for track locations). In the northern GBR (Fig. 9a), waves attenuated by an average of 0.7 m at the reef matrix edge, then generally decreased in height in the lee of the matrix, with a slight increase in height towards the coast likely due to shoaling. In the central GBR where the shelf is wider, waves break at the edge of the reef matrix, then decrease further in height due to friction over the reef matrix. The region in the lee of the reef matrix is deeper and wider than in the north, allowing local generation of wind waves, and possibly wave penetration through spaces in the reef matrix (Fig. 9b). In the southern GBR, there are multiple lagoons between reefs, where there was local generation of wind waves (Fig. 9c).

The wave transmission coefficient (K_T) represents the percentage of H_s transmitted between two locations (Nelson and Lesleighter 1985; Lugo-Fernández et al. 1998) given by:

$$K_T = \frac{H_1}{H_2} \quad (1)$$

where H_1 is significant wave height further offshore; and H_2 is further landward. There was significant scatter in K_T for each of the tracks (Fig. 7b). Although the porosity index (Fig. 7a) increases from north to south along the GBR, there is no clear similar trend when considering K_T (offshore to matrix). There was no statistically significant relationship between the mean porosity of the reef matrix and mean K_T (offshore to lee), with a p value of 0.73 (Fig. 8b). That is, the data do not clearly show that a more porous reef matrix allows significantly larger amounts of wave energy to penetrate the matrix.

There is, however, an increasing trend from north to south in K_T (matrix to lee of matrix). On all tracks, there was an abrupt reduction in mean H_s over the edge of the reef matrix of between 0.5 and 1.2 m, followed by further reduction in H_s as waves travelled over the matrix and into the lee (Fig. 10). There was an increase in H_s in the lee of the matrix due to local wind-wave generation, which occurs mainly from track 6 southwards. This was reflected in K_T (matrix to in the lee of matrix), which was often

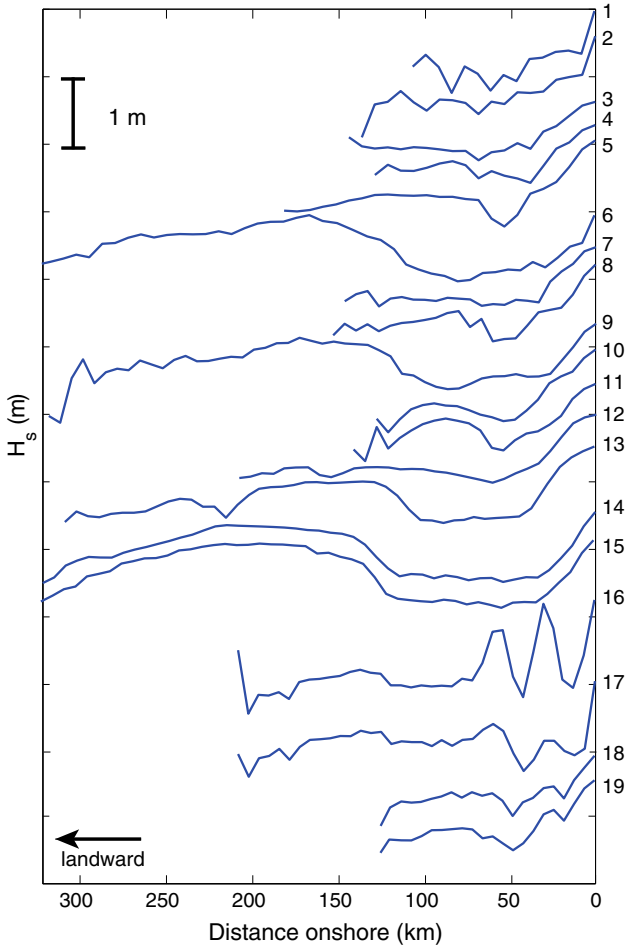

Fig. 10 Mean values of H_s along all tracks from north to south (*top to bottom of plot*). The track number is shown on the *right*. Distance onshore is from the offshore point seaward of the reef matrix for each altimeter pass

greater than 1, and up to 1.6 in the southern GBR (Fig. 7b). These values of K_T (matrix to in the lee of matrix) greater than 1 reflect the process of local generation of wind waves in the GBR lagoon, where H_s increases between offshore and the lagoon.

Incident H_s, wind, and submergence

Figure 11 assesses (1) H_s over the reef matrix as a function of offshore incident wave height and the depth of reef matrix submergence (Fig. 11a), and (2) H_s in the lee of the reef matrix as a function of wind speed and H_s over the reef matrix (Fig. 11b). The depth of reef matrix submergence ranged from 40 to 0.5 m, and offshore incident H_s ranged from 0.2 to 4.5 m (Fig. 11a). For depth of reef submergence greater than approximately 7 m, H_s over the reef matrix was strongly dependent on incident offshore H_s rather than the depth of crest submergence. However, at submergence of <7 m, where more wave breaking and friction decay could be expected, H_s was no longer a function of depth of submergence.

H_s on the reef matrix ranged from 0 to 5 m, and wind speed ranged from <2 to 16 m s^{-1}. There did not appear to be a strong relationship between H_s on the matrix to H_s in the lee of the reef matrix (Fig. 11b). Although very low H_s in the lee of the matrix (<0.5 m) were generally associated with lower H_s on the matrix itself. The highest H_s in the lee of the matrix was more than 2.5 m and occurred during strong winds of more than 13 m s^{-1}, while lower H_s (<0.75 m) mainly occurred during winds of <8 m s^{-1}. That is, H_s in the lee of the reef matrix is related largely to the local wind speed, indicating the local generation of the wave field in the lee of the reef matrix.

Discussion

The present research represents the first comprehensive, large-scale study, of the influence of an offshore reef system on wave climate and wave transmission. Previous studies concentrated largely on wave transmission over individual reefs. Such studies indicated that over individual reefs, wave conditions are strongly depth dependent (Young 1989; Hardy et al. 1990, 1991). However, the present research shows that within the GBR matrix the wave climate is not strongly dependent on reef submergence. It is clear that for depth of reef submergence less than approximately 7 m, there is significant attenuation of wave energy by the reef matrix, but no clear functional dependence on depth <7 m.

A similar situation occurs for reef matrix porosity. There is no clear evidence to suggest that as porosity decreases, wave attenuation increases. These two outcomes may seem counter intuitive, but are broadly consistent with previous studies. Young and Hardy (1993) showed that there was strong tidal modulation of wave height on individual reefs but not between such reefs. Similarly, satellite data reported by Young (1999) indicated that the wave shadow cast by islands is much larger the size of the island itself.

The present data show that although the extent of initial wave breaking at the seaward edges of isolated reefs may be strongly depth dependent (Hardy et al. 1990, 1991), by the time subsequent bottom friction decay has further impacted waves, the wave energy that penetrates such reefs has little depth modulation. That is, at low depth of submergence, the attenuation will be mainly depth-limited breaking at the seaward edge of the reef. At greater depths of submergence, there will be some breaking at the reef edge but then greater decay due to bottom friction across the hydrodynamically rough coral bottom. The net result is that there is not a strong dependence on depth of submergences in the lee of these isolated reefs.

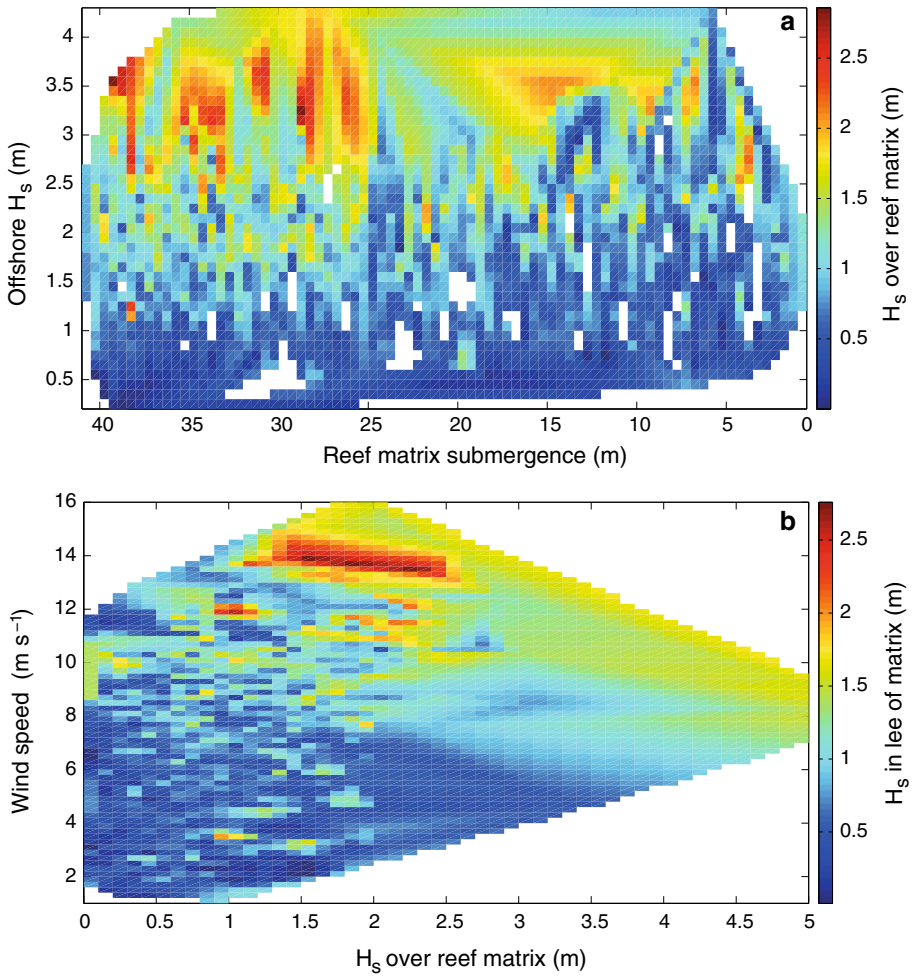

Fig. 11 **a** H_s in the lee of the reef matrix as a function of depth of submergence of the crest and incident H_s; and **b** H_s in the lee of the matrix as a function of H_s at the matrix and wind speed

The individual reefs themselves, just like islands, appear to cast a wave shadow much larger than the reef itself. Thus, a matrix of isolated reefs is remarkably effective in attenuating wave energy. Hence, the present data shows that wave conditions landward of the reef matrix are not strongly dependent on the porosity of the matrix (Fig. 8b).

This weak dependence of transmitted wave energy on depth of reef submergence and reef porosity was also evident in data landward of the GBR matrix. Here, wave conditions depend largely on the local wind rather than wave conditions either seaward or within the GBR matrix (Fig. 11b). This is because the GBR is a very effective wave absorber, irrespective of water depth and reef porosity.

These results have important implications for wave modelling near reef systems. Models which consider isolated reefs as near point wave absorbers may underestimate the wave attenuation potential of the full reef matrix. Although made up of individual, apparently isolated reefs, the full matrix acts to attenuate the majority of incident energy, for most commonly occurring depths of reef submergence. Thus, as previously shown by Murray and Ford (1983), wave conditions landward of the GBR and presumably other reef systems are largely composed of locally generated wind waves. The amount of energy penetrating the seaward reef matrix is relatively minor.

Acknowledgments The authors wish to thank C. Bosserelle for assistance with GMT calculations; P. Cipollini for useful discussions about satellite altimetry; Project 3DGBR (James Cook University) for the bathymetry of the Great Barrier Reef; the altimeter data were derived as part of two projects funded by the Australian Research Council (ARC LP0882422; DP1301002150). R. Ranasinghe's contribution to this research was partly supported by the AXA Research Fund and the Deltares Coastal Maintenance Research Programme 'Beheer & Onderhoud Kust'. This support is gratefully acknowledged.

References

Angwenyi C, Rydberg L (2005) Wave-driven circulation across the coral reef at Bamburi Lagoon, Kenya. Estuar Coast Shelf Sci 63:447–454

Beaman R (2010) Project 3DGBR: a high-resolution depth model for the Great Barrier Reef and Coral Sea. Project 2.5i.1a Milestone 10 June 2010. Marine and Tropical Sciences Research Facility, Reef and Rainforest Research Centre

Chelton DB, Walsh EJ, MacArthur JL (1989) Pulse compression and sea level tracking in satellite altimetry. Journal of Atmospheric and Oceanic Technology 6:407–438

Dean RG, Dalrymple RA (1991) Water wave mechanics for engineers and scientists. World Scientific Press, Singapore

Dollar SJ (1982) Wave stress and coral community structure in Hawaii. Coral Reefs 1:71–81

Durrant T, Greenslade D, Hemer H, Trenham C (2014) A Global Wave Hindcast focused on the Central and South Pacific. CAWCR Technical, Report No 070

Gallop SL, Bosserelle C, Pattiaratchi C, Eliot I (2012) The influence of coastal limestone landforms on storm erosion and recovery of a perched beach. Cont Shelf Res 47:16–27

Gerritsen F (1981) Wave attenuation and setup on a coral reef. Look Lak Tech Report 48, University of Hawaii, Honolulu

Gourlay MR (1988) Coral cays: products of wave action and geological processes in a biogenic environment. Proc 6th Int Coral Reef Symp 2:491–496

Gourlay MR (1990) Waves, set-up and currents on reefs: cay formation and stability. Proceedings of the Conference on Engineering in Coral Reef Regions, Townsville, pp 149–264

Haigh ID, MacPherson LR, Mason MS, Wijeratne EMS, Pattiaratchi CB, George S (2014a) Estimating present day extreme water level exceedance probabilities around the coastline of Australia: tropical cyclone induced storm surges. Clim Dyn 42:139–157

Haigh ID, Wijeratne EMS, MacPherson LR, Pattiaratchi CB, Mason MS, Crompton RP, George S (2014b) Estimating present day extreme total water level exceedance probabilities around the coastline of Australia: tides, extra-tropical storm surges and mean sea level. Clim Dyn 42:121–138

Hamner WH, Wolanski E (1988) Hydrodynamic forcing functions and biological processes on coral reefs: a status review. Proc 6th Int Coral Reef Symp 1:103–113

Hardy TA, Young IR (1996) Field study of wave attenuation on an offshore coral reef. J Geophys Res 101:14311–14326

Hardy TA, Young IR, Nelson RC, Gourlay MR (1990) Wave attenuation on an offshore coral reef. Proceedings of the 22nd International Conference on Coastal Engineering, ASCE, pp 330–334

Hardy TA, Young IR, Nelson RC, Gourlay MR (1991) Wave attenuation on a coral reef. Australian Civil Engineering Transactions, CE33 1:17–22

Hopley D, Parnell KE, Isdale PJ (1989) The Great Barrier Reef Marine Park: Dimensions and regional patterns. Aust Geogr Stud 27:47–66

Hopley D, Smithers SG, Parnell KE (2007) The geomorphology of the Great Barrier Reef: development, diversity, and change. Cambridge University Press, Cambridge

Kalnay E, Kanamitsu M, Kistler R, Collins W, Deaven D, Gandin L, Iredell M, Saha S, White G, Woollen J, Zhu Y, Leetmaa A, Reynolds B, Chelliah M, Ebisuzaki W, Higgins W, Janowiak J, Mo KC, Ropelewski C, Wang J, Jenne R, Joseph D (1996) The NCEP/NCAR 40-year reanalysis project. Bulletin of the American Meteorological Society 77:437–472

Kistler R, Collins W, Saha S, White G, Woollen J, Kalnay E, Chelliah M, Ebisuzaki W, Kanamitsu M, Kousky V, van den Dool H, Jenne R, Fiorino M (2001) The NCEP-NCAR 50-year reanalysis: monthly means CD-ROM and documentation. Bulletin of the American Meteorological Society 82:247–267

Kono T, Tsukayama S (1980) Wave transformation on reef and some considerations on its application to field. Coastal Engineering in Japan 24:45–57

Lee TT, Black KP (1979) The energy spectra of surf waves on a coral reef. Proceedings of the 16th International Conference on Coastal Engineering, ASCE, pp 588–608

Longuet-Higgins MS, Stewart RW (1962) Radiation stress and mass transport in gravity waves, with application to surf beats. J Fluid Mech 13:481–504

Lowe RJ, Falter JL, Monismith SG, Atkinson MJ (2009) A numerical study of circulation in a coastal reef-lagoon system. J Geophys Res 114:C06022

Lowe RJ, Falter JL, Bandet MD, Pawlak G, Atkinson MJ, Monismith SG, Koseff J (2005) Spectral wave dissipation over a barrier reef. J Geophys Res 110:C04001

Lugo-Fernández A, Roberts HH, Suhayda JN (1998) Wave transformations across a Caribbean fringing-barrier coral reef. Cont Shelf Res 18:1099–1124

Murray RT, Ford LR (1983) Problems in the analysis of data for the assessment of longshore sediment transport: an example from North Queensland. 6th Australian Conference on Coastal and Ocean Engineering, Institution of Engineers Australia, pp 21–26

Nelson RC, Lesleighter EJ (1985) Breaker height attenuation over platform coral reefs. Proceedings of the 7th Australian Conference on Coastal and Ocean Engineering, Institution of Engineers, Australia 1:9–16

Pèquignet AC, Becker JM, Merrifield MA, Boc SJ (2011) The dissipation of wind wave energy across a fringing reef at Ipan, Guam. Coral Reefs 30:71–82

Pickard GL, Andrews JC, Wolanski E (1990) A review of the physical oceanography of the Great Barrier Reef 1976–1986. Australian Institute of Marine Science, Monograph Series, Townsville

Roberts HH (1981) Physical processes on sediment flux through reef-lagoon systems. Proceedings of the 17th International Conference on Coastal Engineering, ASCE, pp 946–962

Saha S, Moorthi S, Pan H-L, Wu X, Wang J, Nadiga S, Tripp P, Kistler R, Woollen J, Behringer H, Liu H, Stokes D, Grumbine R, Gayno G, Wang J, Hou Y-T, Chuang H-Y, Juang H-MH, Sela J, Iredell M, Treadon R, Kleist D, Van Delst P, Keyser D, Derber J, Ek M, Meng J, Wei H, Yang R, Lord S, Van Den Dool H, Kumar A, Wang W, Long C, Chelliah C, Xue Y, Huang B, Schemm J-K, Ebisuzaki W, Lin R, Xie P, Chen M, Zhou S, Higgins W, Zou C-Z, Liu Q, Chen Y, Han H, Cucurull L, Reynolds RW, Rutledge G, Goldberg M (2010) The NCEP Climate Forecast System Reanalysis. Bulletin of the American Meteorological Society 91:1015–1057

Storlazzi CD, Ogston AS, Bothner MH, Field ME, Presto MK (2004) Wave- and tidally-driven flow and sediment flux across a fringing coral reef: Southern Molokai. Hawaii. Cont Shelf Res 24:1397–1419

Symonds G, Black KP, Young IR (1995) Wave-driven flow over shallow submerged reefs. J Geophys Res 100:2639–2648

Tolman HL (1991) A third-generation model for wind waves on slowly varying, unsteady and inhomogeneous depths and currents. J Phys Oceanogr 21:782–797

Tolman HL (2008) A mosaic approach to wind wave modeling. Ocean Model 25(1-2):35–47

Tolman HL (2009) User manual and system documentation of WAVEWATCH III version 3.14. NOAA / NWS / NCEP / MMAB Technical Note 276, 194 pp

Wolanski EF (1986) Observations of wind-driven surface gravity waves offshore from the Great Barrier Reef. Coral Reefs 4:213–219

Young IR (1989) Wave transformation over coral reefs. J Geophys Res 74:9779–9789

Young IR (1999) Seasonal variability of the global ocean wind and wave climate. International Journal of Climatology 19:931–950

Young IR, Hardy TA (1993) Measurement and modelling of tropical cyclone waves in the Great Barrier Reef. Coral Reefs 12:85–95

Young IR, Zieger S, Babanin AV (2011) Global trends in wind speed and wave height. Science 332:451–455

Young IR, Babanin AV, Zieger S (2013) The decay rate of ocean swell observed by altimeter. J Phys Oceanogr 43:2322–2333

Zieger S, Vinoth J, Young IR (2009) Joint calibration of multi-platform altimeter measurements of wind speed and wave height over the past 20 years. Journal of Atmospheric and Oceanic Technology 26(12):2549–2564